ELSEVIER

Polymer 40 (1999) 4543–4551

polymer

Isothermal thickening and thinning processes in low molecular weight poly(ethylene oxide) fractions crystallized from the melt 6. Configurational defects in molecules

E.-Q. Chen[a], S.-W. Lee[a], A. Zhang[a], B.-S. Moon[a], P.S. Honigfort[a], I. Mann[a], H.-M. Lin[a], F.W. Harris[a], S.Z.D. Cheng[a,*], B.S. Hsiao[b], F. Yeh[b]

[a]*The Maurice Morton Institute and Department of Polymer Science, The University of Akron, Akron, OH 44325-3909, USA*
[b]*Department of Chemistry, The State University of New York at Stony Brook, Stony Brook, NY 11794-3400, USA*

Dedicated to Professor Ronald K. Eby on the occasion of his 70th birthday

Received 9 September 1998; received in revised form 21 October 1998; accepted 23 October 1998

Abstract

Three two-arm poly(ethylene oxide) (PEO) fractions were prepared via a coupling reaction. These PEOs possess the same number average molecular weight of 2220 g mol^{-1} for each arm and the coupling agents used are *para*-(1,4-), *meta*-(1,3-) and *ortho*-(1,2-) benzene dicarbonyl dichlorides. The configurations of these two-arm PEO molecules thus exhibit angles of 180, 120 and 60°, respectively, at the coupling agent. These coupling agents may substantially affect the overall molecular conformations (OMCs) in the crystals of the two-arm PEOs. Wide angle X-ray diffraction powder patterns indicate that these fractions have the same crystal structure regardless of the coupling agents (which act as defects) used, and therefore the defects must be excluded from the lamellar crystals. Differential scanning calorimetry results show that two populations of crystals exist when the samples are crystallized at relatively low undercoolings. This is particularly evident in the cases of 1,4- and 1,3-two-arm PEOs. Corresponding small angle X-ray scattering experiments show two different long periods in these fractions. Experimental results reveal the possibility that the crystals which correspond to the thinner long period possess an extended OMC in which one layer of defects exists between two neighboring lamellae. The crystals which exhibit the thicker long period possess a once-folded OMC, with two layers of defects lying between neighboring lamellae. During heating, the extended OMC crystals with the thinner long period melt at lower temperatures than the thicker, once-folded OMC crystals. Detailed studies on the efforts of these configurational defects on the lamellar crystal morphology and crystal stability are discussed in the main body of the article.

Keywords: Poly(ethylene oxide); X-ray diffraction and scattering; Configurational defect

1. Introduction

Polymer crystallization has been extensively studied for the past fifty years and many researchers have provided new findings which have added to our understanding of this stimulating topic. Over the past eight years, we have published a series of experimental observations on low molecular weight (LMW) poly(ethylene oxide) (PEO) fractions. An initial transient state which is seen during the crystallization of those fractions has been recognized as consisting of non-integral folded chain (NIF) crystals [1,2]. This transient state occurs prior to the formation of the final integral folding chain (IF) crystals [3–6]. We have also carried out several steps towards understanding the effects of molecular architecture on the crystallization behavior of LMW PEOs. These include the molecular weight dependence [7], the end group effect [8], and the effect of chain defect [9] on the thickening and thinning processes both in the initial stage of crystallization and those following crystallization.

Crystalline polymers are self-assembling systems with strong molecular interactions. Through research on this subject, we hope to understand the self-assembly mechanism on a molecular scale via the study of specifically designed molecular architectures. In one of our previous publications, we reported the crystallization behavior of two two-arm PEOs in which the arms (molecular weights

* Corresponding author. Tel.: +1-330-972-6931; fax: +1-330-972-8626.
E-mail address: cheng@polymer.uakron.edu (S.Z.D. Cheng)

0032-3861/99/$ - see front matter
PII: S0032-3861(99)00069-5

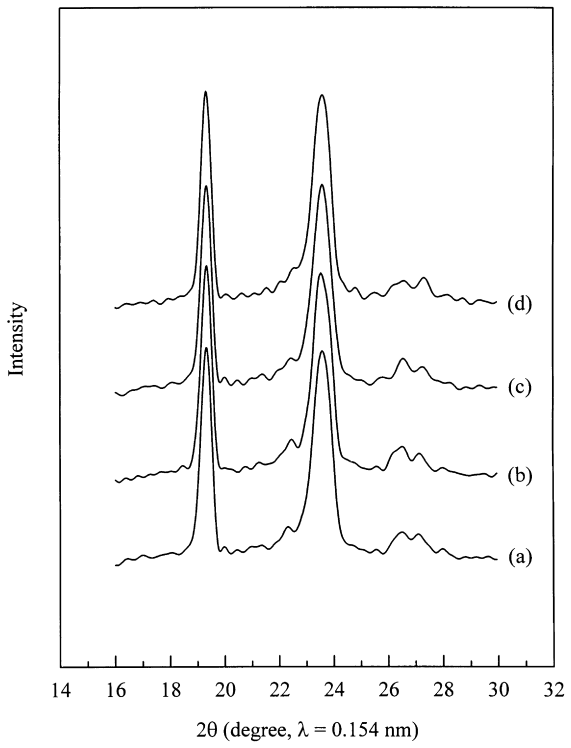

Fig. 1. WAXD powder patterns for the two-arm PEOs and linear PEO with the same molecular length as that of a single arm: (a) linear PEO, (b) 1,4-two-arm, (c) 1,3-two-arm, and (d) 1,2-two-arm PEO. The crystallization temperatures was 48°C for all the samples.

of 2300 and 5500 g mol^{-1}) were linked by *para*-benzene dicarbonyl dichloride [9].

In this study, three two-arm PEO fractions were prepared via coupling reactions. These PEOs possess the same number average molecular weight (M_n) of 2220 g mol^{-1} for each arm and the coupling agents (which act as defects) used were *para*-(1,4-), *meta*-(1,3-) and *ortho*-(1,2-) benzene dicarbonyl dichlorides. These two-arm PEO molecules thus form angles of 180°, 120° and 60°, respectively, at the centers. We speculated in Ref. [9] that 1,4-two-arm PEO crystals may possess two types of overall molecular conformations (OMCs): an extended and a once-folded OMC. The difference between these two crystalline OMCs is that when the crystals consist of the extended OMC only one layer of defects is located between neighboring lamellae, while for crystals formed with the once-folded OMC, two layers of defects exist between neighboring lamellae.

In this article, a detailed analysis of the experimental results will support the possibility that two different OMCs exist in these two-arm PEOs. At relatively low undercoolings, such as at a crystallization temperature of 48°C (corresponding roughly to an undercooling of less than 10°C), nanoscopically separated crystals may be formed with only one type of OMC at least in the cases of 1,4- and 1,3-two-arm PEOs. Therefore, the individual characteristics of these OMCs can be detected through experimental observations.

2. Experimental section

2.1. Material synthesis and characterization

Three two-arm PEO fractions were synthesized via coupling reactions in chloroform using 1,4-, 1,3-, and 1,2-benzene dicarbonyl dichloride as coupling agents. These coupling agents were obtained from Aldrich. A LMW PEO fraction [α,ω-methoxy-hydroxy-poly(ethylene oxide)] (HO–$(CH_2CH_2O)_n$–CH_3) with a molecular weight of 2220 g mol^{-1} was also purchased from the same company. Further fractionation was carried out in our laboratory. The PEO used possesses one hydroxyl and one methoxy end group. The linear PEO fraction and coupling agents were first dried under vacuum and later freeze-dried in dry benzene. Detailed procedures of the coupling reaction and the separation of the two-arm PEOs from their parent PEO fraction have been published earlier [9].

Gel permeation chromatography (GPC) experiments were carried out in tetrahydrofuran (THF) at 30°C to determine the number average MW and polydispersities of the two-arm PEOs. GPC was also used to examine each fraction during the fractionation procedure. The effective MW range for the columns used was 500–600 000 g mol^{-1}. The GPC was calibrated using standard linear PEO fractions in the same MW range. Fourier transform infrared spectroscopy (FTIR, Mattson Galaxy 5020) measurements were carried out in the range of 500–4000 cm^{-1} to analyze the end groups and the coupling agents of the PEOs. The films of linear and two-arm PEO fractions were solution-cast on NaCl pellets for FTIR measurements. A Knauer vapor pressure osmometer (VPO) was used to determine the number average MW of the fractionated linear PEO and two-arm PEOs in toluene at 40°C. The VPO was calibrated using sucrose octaacetate in toluene. The concentrations of the sample solutions (g kg^{-1}) were identical to that of the calibration solution. Light scattering (LS) experiments were conducted to insure the accuracy of the polydispersities by measuring the weight average MWs.

2.2. Equipment and experiments

Differential scanning calorimetry (DSC, TA2000 system) experiments were carried out to study the isothermal crystallization and the melting behavior of these linear and two-arm PEOs. The DSC was calibrated with *p*-nitrotoluene, naphthalene, and indium standards. The sample weight was maintained at approximately 0.5 mg and the pan weights were kept a constant to within ± 0.001 mg. Isothermal crystallization was conducted by quenching the samples from the isotropic melt to a preset crystallization temperature (T_c). In the low undercooling range a self-seeding technique, which has been described previously, was used for the isothermal crystallization [10–14]. After annealing at the self-seeding temperature T_s($T_s = T_m - 1.5$°C) for 20 min, the samples were quickly shifted to the preset

Table 1
Molecular characteristics of linear and two-arm PEO fractions

	M_n[a]	M_n[b]	M_w/M_n[c]	M_a[d]	Average length (nm)[e]
Linear PEO	2200	2220	1.02	—	14.0
1,4-two-arm PEO	4500	4550	1.05	2220	29.0
1,3-two-arm PEO	4500	4550	1.05	2220	29.0
1,2-two-arm PEO	4490	4550	1.05	2220	29.0

[a] Number average molecular weight from GPC.
[b] Number average molecular weight from VPO.
[c] Polydispersities from GPC, and independently checked via light scattering by measuring the weight average MWs.
[d] Number average molecular weight of each arm.
[e] The average chain lengths of the linear fractions were calculated from the equation: $\ell = M_n/d$, ($d = 158.2[10–14]$). For the two-arm PEO fractions, the average chain lengths were calculated by doubling the linear fraction length and adding the size of the coupling agent.

isothermal T_c. The crystallized samples were then heated to above the melting temperature at a heating rate of 5°C min^{-1}.

Time-resolved synchrotron wide angle X-ray diffraction (WAXD) and small angle X-ray scattering (SAXS) experiments were simultaneously conducted at the synchrotron X-ray beam line X27C of the National Synchrotron Light Source at Brookhaven National Laboratories. The wavelength of the X-ray beam was 0.1307 nm. As common WAXD patterns obtained using CuKα radiation possess a wavelength of 0.154 nm, the synchrotron radiation wavelength was converted into the CuKα radiation wavelength in the WAXD plot (see later in Fig. 1). Isothermal crystallization measurements were carried out on a customized two-chamber hot stage. The temperature was controlled to within ± 0.5°C. A heating rate of 0.5°C min^{-1} was used to study the crystal melting behavior of the samples after isothermal crystallization. Position sensitive proportional counters were used to record the scattering and diffraction patterns. The SAXS counter was calibrated with a duck tendon which exhibits scattering peaks at $q = 0.109$, 0.22, 0.33 nm^{-1} etc. ($q = 4\pi\sin\theta/\lambda$, where λ is the wavelength of the synchrotron X-ray radiation). The Lorentz correction was performed by multiplying the intensity, I (counts per second), by q^2. The WAXD counter was calibrated using silicon crystals of a known crystal size.

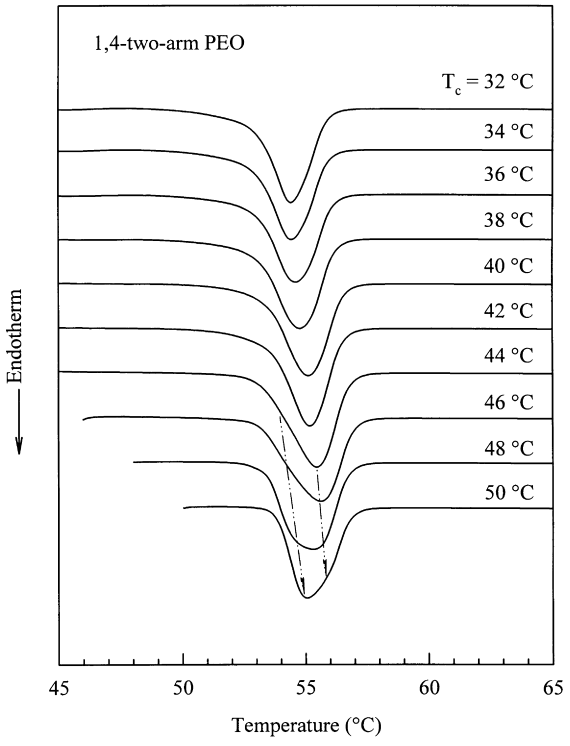

Fig. 2. A set of DSC heating curves obtained at a rate of 5°C min^{-1} for 1,4-two-arm PEO after isothermal crystallization at different temperatures in the region from 32 to 50°C.

3. Results

3.1. Material analysis and characterization

The linear and two-arm PEOs were analyzed using several molecular characterization methods. After the coupling reaction, there remains a mixture of the linear ''parent'' and the two-arm PEO molecules. Therefore, it is necessary to carefully separate these two components via fractionation. Table 1 lists the analytical results for M_n and MW distribution as measured by GPC and VPO after this fractionation. The samples possessed narrow MW distributions, and therefore should serve as good model systems to study polymer crystallization. FTIR was also used to examine the linear and two-arm PEOs. The two-arm PEOs do not possess the absorption band at 3500 cm^{-1} which is seen in linear PEO. This absorption band originates from hydrogen bonding and the OH stretching vibration. However, the vibration bands which correspond to the phenylene and carbonyl groups can be observed in two-arm PEO samples at 1720 and 1600 cm^{-1}, respectively [9].

Fig. 1 shows a set of WAXD patterns for the three two-arm PEOs and the linear PEO ($M_n = 2220$) after both were crystallized at 48°C for a prolonged time (e.g. a few days to a week). All patterns exhibit the same 2θ reflections. This indicates that the two-arm PEO samples possess crystal structures identical to that of the linear PEO (specifically, a monoclinic unit cell with $\beta = 129°$ [15]). It is thus evident that the defects in these two-arm PEOs are not able to destroy the PEO chain packing of the monoclinic structure. This may be due to the fact that the defects are excluded from the crystals and are located in the amorphous regions between lamellae. The crystallinities of these samples can also be determined from Fig. 1. Linear PEO shows the highest crystallinity at 92–95%, and the three two-arm PEOs exhibit crystallinites similar to each other at 83–85% following a weight correction for the coupling agents (4%). Therefore, there is approximately a 10% difference

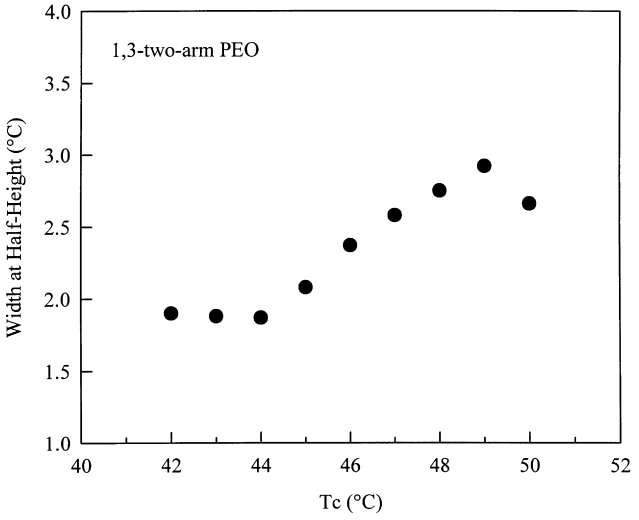

Fig. 3. The change of the width at half-height of the endothermic peak of the 1,3-two-arm PEO (obtained at a heating rate of 5°C min^{-1}) with changing isothermal crystallization temperatures.

in crystallinity between the linear and two-arm PEO samples.

3.2. Crystal melting as observed by differential scanning calorimetry

Fig. 2 shows a set of DSC heating curves for the 1,4-two-arm PEO after it was isothermally crystallized at several T_cs between 32 and 50°C. From this, it can be seen that the peak temperatures of the major endotherms remain nearly constant at 54.5°C for crystallization temperatures below 38°C. The peak temperature of the major endotherm gradually increases with increasing crystallization temperature for $T_c > 38$°C. When the T_c exceeds 44°C, the melting peak broadens. At the same time, a shoulder develops on the lower temperature side of the melting peak and eventually two endotherms can be clearly recognized. The melting behavior of the 1,3-two-arm PEO is similar to the 1,4-two-arm PEO. Its melting peak also exhibits a broadening at T_cs $>$ 44°C which may be attributed to two populations of crystals. Fig. 3 shows the change in the width at half-height of the endothermic peaks for the 1,3-two-arm PEO with changing isothermal crystallization temperature. It is obvious that at relatively low T_cs the width at half-height is equal to or narrower than 1.9°C. Above $T_c = 44$°C, the width at half-height starts to broaden and reaches 3.0°C at $T_c = 49$°C. The width slightly decreases above $T_c = 49$°C. In the case of the 1,2-two-arm PEO, a shoulder can be seen on the low temperature side of the melting peak at T_c above 44°C. However, this shoulder does not develop extensively.

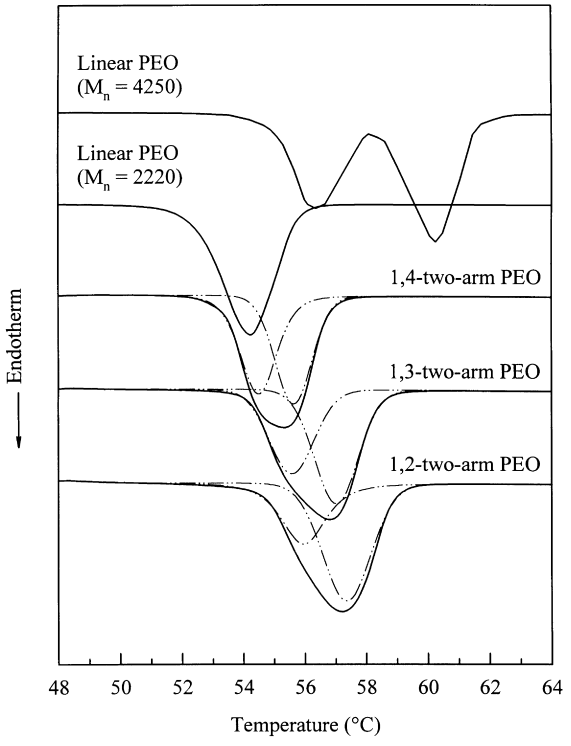

Fig. 4. A set of DSC heating curves for the 1,4-, 1,3- and 1,2-two-arm PEOs after crystallization at 48°C. Heating curves of the linear PEO ($M_n = 2220$) and PEO ($M_n = 4250$) are also included for comparison. The heating rate was 5°C min^{-1}.

Extensive study was done on two-arm PEO crystals grown at 48°C. Fig. 4 shows the melting curves of the two-arm PEOs after they were crystallized at 48°C for prolonged crystallization times. The melting curves of the linear ''parent'' PEO ($M_n = 2220$) and PEO ($M_n = 4250$) are also included in Fig. 4 for comparison. Only a single melting endotherm (54.5°C) is found for the linear PEO ($M_n = 2220$), and it is constant over the whole T_c range. This melting endotherm is sharp and its width at peak half-height is less than 2.0°C at a heating rate of 5°C min^{-1}. The sharpness of this melting peak is similar to that observed in organic small molecules and *n*-alkanes. The linear PEO ($M_n = 4250$) possesses a molecular weight close to that of the two-arm PEOs, and its DSC heating curve reveals two major melting endotherms at approximately 57 and 61°C after prolonged crystallization times [5]. However, it can be seen that the melting behaviors of the two-arm PEOs are different from that of both of the linear samples. The melting peak temperatures of these two-arm PEOs are higher than that of the linear PEO ($M_n = 2220$). As opposed to their melting curves at low T_cs (see Fig. 2), the melting peak of the two-arm PEOs after crystallization at 48°C (Fig. 4) may be considered to be composed of two overlapped melting endotherms (see also Fig. 3). This is particularly evident in the cases of the 1,4- and 1,3-two-arm PEOs. When the two-arm-PEO samples are isothermally crystallized at 48°C, their two melting peak temperatures are very close. They are 55.6 and 54.5°C for the 1,4-two-arm PEO, 57.0 and 55.5°C for the 1,3-two-arm PEO, and 57.4 and 56.0°C for the 1,2-two-arm PEO.

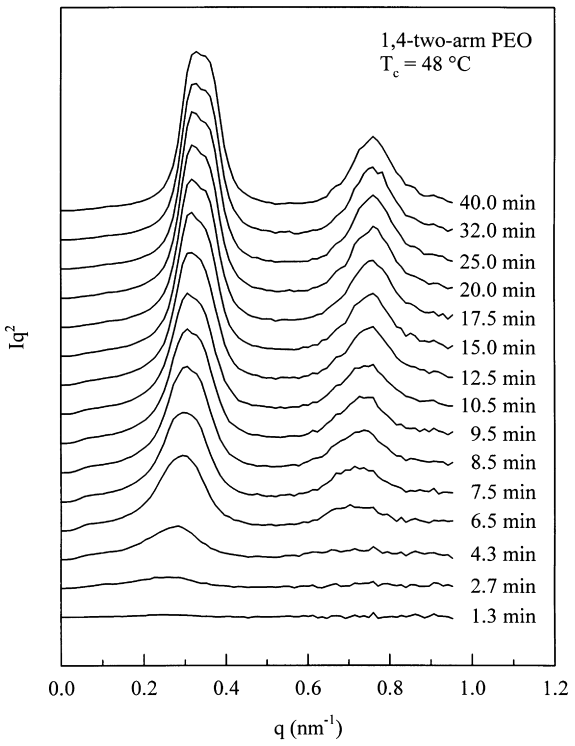

Fig. 5. A set of real-time resolved synchrotron SAXS results for the 1,4-two-arm PEO isothermally crystallized at 48°C. The curves are presented after the Lorentz correction.

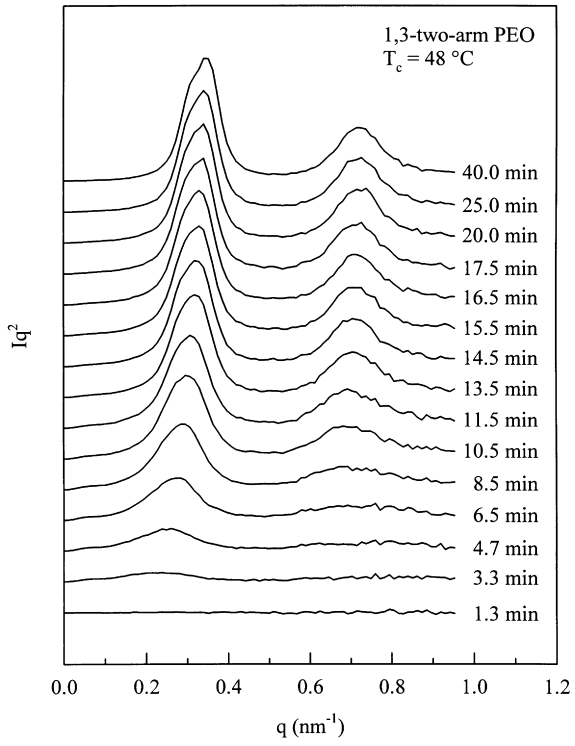

Fig. 6. A set of real-time resolved synchrotron SAXS results for the 1,3-two-arm PEO isothermally crystallized at 48°C. The curves are presented after the Lorentz correction.

3.3. Isothermal crystallization behavior as observed by small angle X-ray scattering

Figs. 5–7 show the real-time resolved synchrotron SAXS results obtained during isothermal crystallization of the three two-arm PEO fractions at T_c = 48°C utilizing the self-seeding process [10–14]. It is evident from Fig. 5 that the initial long period of the 1,4-two-arm PEO is 24.0 nm. The broad scattering peak increases in intensity with increasing isothermal crystallization time and the peak position shifts to higher q values (an apparent thinning process). This broad scattering peak gradually grows into two separated peaks which can clearly be recognized after a crystallization time of 8 min. The long periods corresponding to these two peaks decrease slightly with prolonged crystallization times, reaching values of 19.8 and 17.3 nm. A similar observation was made in the case of the 1,3-two-arm PEO as is shown in Fig. 6. The long period at the onset of crystallization is approximately 26.0 nm. After about 10 min of crystallization, a shoulder develops on the low q side of the low q scattering peak. The long periods of these two peaks decrease to 20.2 and 17.5 nm, much like the 1,4-two-arm PEO. In the case of the 1,2-two-arm PEO, which is shown in Fig. 7, an apparent thinning process is also observed. The initial long period of approximately 26.0 nm gradually decreases to 20.4 nm with increasing crystallization time. However, the scattering peak shows only a relatively broad maximum which remains in evidence even after crystallization is complete.

In brief, as observed by synchrotron SAXS, the two-arm PEOs exhibit similar isothermal crystallization behavior with an apparent thinning process at T_c = 48°C. This behavior differs from that of the linear PEO (M_n = 4250), which exhibits not only a thinning but also a thickening process during isothermal crystallization. For example, an initial SAXS peak with a long period of 16.2 nm is found for the linear PEO (M_n = 4250) crystallized at 48°C. This long period gradually shifts to a q value of 13.7 nm, corresponding to a thinning process. Meanwhile, another scattering peak develops at 25.0 nm, corresponding to a thickening process [5].

The developments in the SAXS patterns shown in Figs. 5–7 are also different from that of the linear PEO (M_n = 2220). It is found that the linear PEO (M_n = 2220) maintains a constant long period of 14.8 nm during isothermal crystallization at 48°C. Fig. 8 presents a set of SAXS experimental results at the final stages of crystallization for the linear PEO (M_n = 2220) and the three two-arm PEOs crystallized at 48°C. In the case of the linear PEO, the first-order scattering maximum appears at 14.8 nm and other maxima exist up to at least the sixth-order (only the first- and second-orders are shown in Fig. 8(a)). It can be seen that the scattering of the first-order peak is very sharp, wherein the width of the peak at the half-height corresponds to a correlation length of approximately 500 nm along the normal of the lamellar surface. For the two-arm PEOs, the long periods are greater

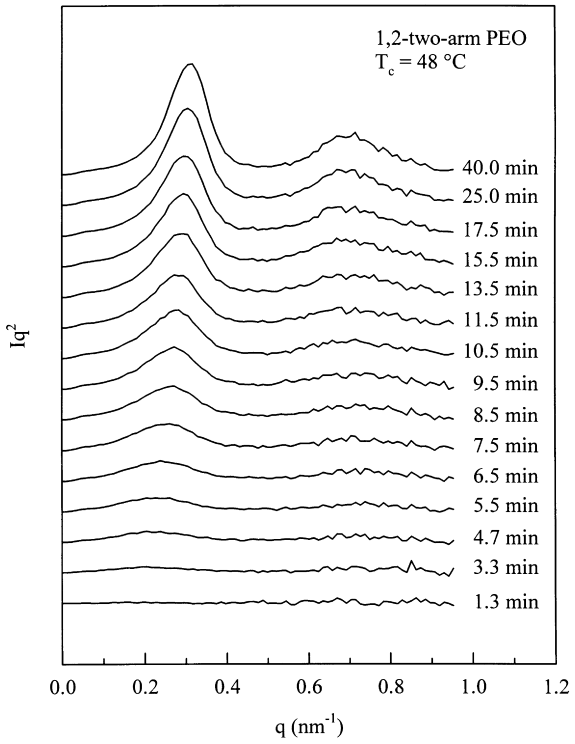

Fig. 7. A set of real-time resolved synchrotron SAXS results for the 1,2-two-arm PEO isothermally crystallized at 48°C. The curves are presented after the Lorentz correction.

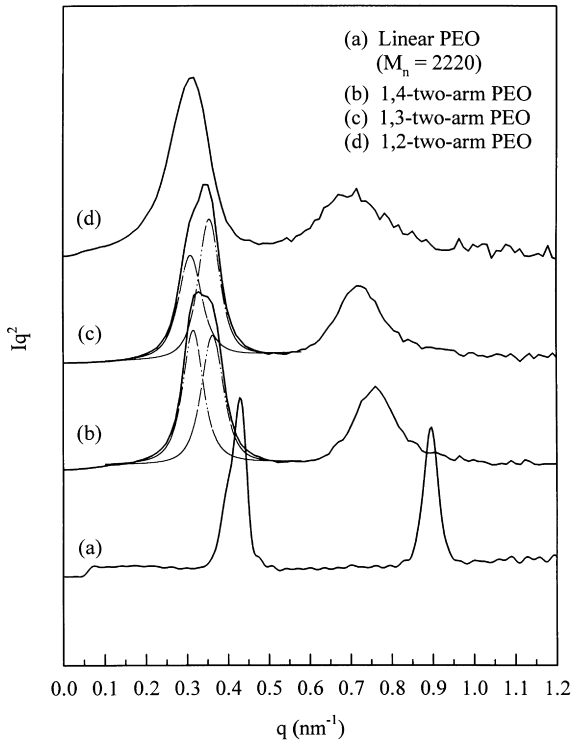

Fig. 8. Four real-time synchrotron SAXS curves for linear and two-arm PEOs after complete crystallization: (a) linear PEO, (b) 1,4-two-arm, (c) 1,3-two-arm, and (d) 1,2-two-arm PEOs. The linear PEO has a same molecular length as that of a single arm. All the samples were isothermally crystallized at 48°C. The curves are presented after the Lorentz correction.

than that of the linear PEO (M_n = 2220). Fig. 8(b) and (c) show the scattering peaks resulting from the peak separation of the first-order scattering maximums in the cases of the 1,4- and the 1,3-two-arm PEO, respectively. This phenomenon indicates that there should be two nanoscopically separated populations of lamellar crystals with two different long periods in these two-arm PEOs. The correlation lengths of the two long periods obtained by peak separation are found to be approximately180 nm for both the 1,4- and 1,3-two-arm PEOs. In the case of the 1,2-two-arm PEO, there is no evidence from either Fig. 7 or Fig. 8(d) that the sample possesses two lamellae stacking populations. The correlation length of this fraction is determined to be 100 nm.

4. Discussion

4.1. Two overall molecular conformations in two-arm poly(ethylene oxides)

It is known that LMW PEO fractions crystallized from the melt at low undercooling form IF crystals [10–14]. The OMCs of PEO chains in this crystalline state are either extended, once-folded, twice-folded or triply-folded, etc. However, the linear PEO (M_n = 2220) can only grow extended chain crystals [9]. The average molecular length of this linear PEO fraction with a 7/2 helix conformation is 14.0 nm (see Table 1), and thus the measured long period of 14.8 nm consists of the chain length and an inter-lamellar region of 0.8 nm. This indicates an extended OMC. Therefore, the melting temperature of 54.5°C for this linear PEO is associated with the melting of extended chain crystals. It has been reported that the linear PEO (M_n = 4250) may form crystals with extended and once-folded OMCs when the T_c ranges from 36 to 55°C [5]. The sample shown in Fig. 4 was crystallized in this temperature range, and two melting temperatures can be seen. As a result of the fact that the lamellar thickness of the extended chain crystal is almost twice that of the once-folded chain crystal, the higher melting temperature is attributed to the extended chain crystals and the lower one to the once-folded chain crystals.

It is speculated that the two-arm PEOs studied may also possess both the extended and the once-folded OMCs when the molecules crystallize at low undercoolings. However, the coupling agents located at the chain center act as configurational defects (chemical defects). It is interesting to see how these defects affect the chain packing when the two-arm PEOs crystallize. In the case of two-arm PEO crystals with the once-folded OMC, the two arms of each molecule are packed into the same lamella, excluding the defects from the crystals by locating them on the top and bottom surfaces of the lamella. The morphology of the two-arm PEO crystals with the once-folded OMC is thus similar to that of the once-folded chain crystals in the linear PEOs, despite the fact that the fold of the two-arm PEO crystals contains the defects, which may in turn affect the lamellar packing and

the fold surface free energy. However, two-arm PEOs with the extended OMC exhibit different lamellar thickness and arrangement from that of this linear counterpart. Instead of forming a single lamella with a lamellar thickness corresponding to the extended chain length, the two arms of each PEO molecule are crystallized into two neighboring lamellae, causing the defects to be located between these lamellae. As a result, the lamellar thickness of the crystals is close to half that of the chain contour length, which is in turn nearly identical to the thickness of the linear PEO crystals with the once-folded OMC. The melting of these two types of crystals, as observed by DSC, and the presence of two long periods, as observed by SAXS experiments, provide evidence of two-arm PEO crystals with extended and once-folded OMCs when crystallized at low undercoolings.

4.2. Crystal morphologies of two-arm poly(ethylene)oxides

During the isothermal crystallization of linear LMW PEO, NIF crystals appear as a transient state followed by thinning and thickening processes [1–9]. In the case of the two-arm PEOs looked at in this study, the NIF crystals may also initially form because of kinetic reasons even though they are thermodynamically less stable than IF crystals [16,17]. It is interesting that only an apparent thinning process is observed when these two-arm PEOs crystallize. There may be two aspects that explain this process. First, NIF crystals possess a long period greater than that of crystals with the once-folded OMC. The thinning process is thus required to transform the NIF to once-folded crystals. Second, during the formation of crystals with extended OMC, each two-arm PEO chain must to be extended in order to participate in two neighboring lamellae. During this process, the defects at the chain center diffuse towards the inter-lamellar region between the two neighboring lamellae in order to maximize the crystallinity (and thus, the stability). An amorphous layer is thus formed consisting of these defects. This process leads to a decrease of the long period, resulting in an apparent thinning behavior.

Comparing the crystals of these two different OMCs in the two-arm PEOs, it is reasonable that the crystals with the once-folded OMC have a greater long period than that of the crystals formed at the same crystallization temperature with an extended OMC. This is due to the fact that the once-folded OMC crystals possess both an upper and lower defect layer on each lamella whereas the extended OMC crystals possess only one layer of defects which exists between the neighboring lamellae. Note that the crystals of the 1,4- and 1,3-two-arm PEOs crystallized at 48°C show that the evolution of the two long periods becomes obvious in the middle stage of crystallization (Figs. 5 and 6). The long period of the 1,2-two-arm PEO crystals is very close to the larger long period in the 1,4- and 1,3-two-arm PEOs. Hence, the long period of the 1,2-two-arm PEO may correspond to crystals with the once-folded OMC. However, as this scattering peak is relatively broad, it may also possibly include some extended OMC crystals. For this reason, we expect that this long period does not represent nanoscopically separated crystals with specific OMCs, but rather a mixture of crystalline OMCs.

However, compared to the long period of 14.8 nm for the linear PEO ($M_n = 2220$), the 1,4-two-arm PEO exhibits significantly greater long periods when crystallized at 48°C (17.3 and 19.8 nm). If we assume that the long period of 17.3 nm corresponds to 1,4-two-arm PEO crystals with the extended OMC, the difference between this long period (17.3 nm) and that of the linear PEO $M_n = 2220$) is 2.5 nm. As the long period of the two-arm PEO with the extended OMC includes one layer of defects, the 2.5 nm difference may be attributed to the thickness of this defect layer. Moreover, the difference between the larger long period of 19.8 nm (which is assumed to correspond to 1,4-two-arm PEO crystals with the once-folded OMC) and that of the crystals in the linear PEO ($M_n = 2220$) is 5.0 nm. As the long period of the 1,4-two-arm PEO crystals with the once-folded OMC contains two defect layers, each defect layer must therefore occupy 2.5 nm. It is also found that the value of 2.5 nm is consistent with the difference between the larger and smaller long periods exhibited by the 1,4-two-arm PEO at the same T_c ($19.8 - 17.3 = 2.5$ nm, which corresponds to the thickness of the added defect layer). A similar comparison can be made between the 1,3-two-arm and linear ($M_n = 2220$) PEOs. The difference between the smaller long period of 17.5 nm for the 1,3-two-arm PEO and that of the linear PEO fraction is 2.7 nm, while the difference between the larger long period of 20.2 nm for the 1,3-two-arm PEO and the long period of the linear PEO is 5.4 nm. Each defect layer is thus 2.7 nm thick. This value also matches well with the difference between the larger and smaller long periods within this fraction ($20.2 - 17.5 = 2.7$ nm). In the case of 1,2-two-arm PEO, the only comparison which can be made is the difference between its single long period (20.4 nm) and that of the linear PEO. This difference is 5.6 nm, and therefore the thickness of each defect layer in the 1,2-two arm PEO is approximately 2.8 nm.

Based on a computer simulation, the defect thickness of the two-arm PEOs in the extended OMC is approximately 1 nm (including the ester groups). It appears reasonable to speculate that the defects in this OMC cannot exactly arrange themselves into a single layer with this thickness because of space restrictions caused by the lateral packing of the PEO chain into the crystals (on the a*b-plane of the PEO crystals). Surface enhanced Raman scattering experiments reveal that the benzene ring of the coupling agents are perpendicular to the fold surface [18]. Therefore, the defects likely have to adjust their neighboring positions up or down with respect to the lamellar surface normal in order to accommodate this conformational restriction. This, in turn, results in an increase of the defect layer thickness. Moreover, any additional PEO repeat units are not incorporated in the crystals, but instead must remain in the

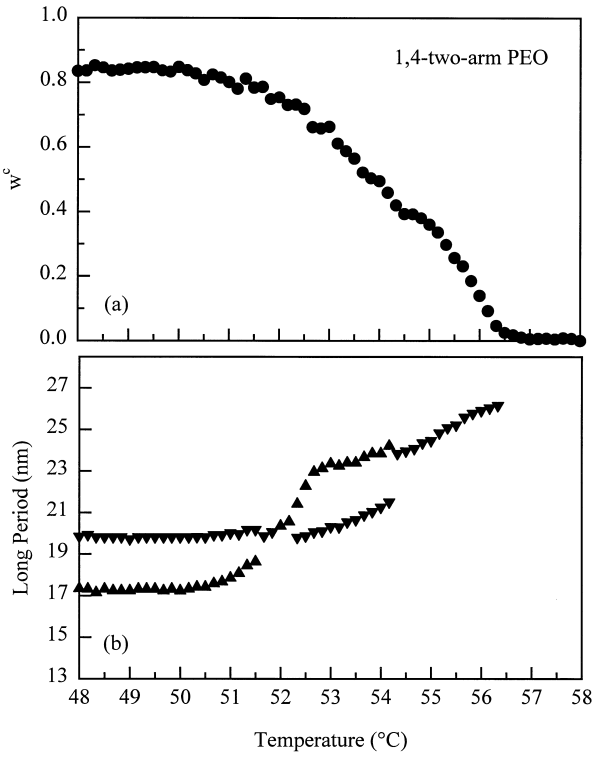

Fig. 9. Changes in crystallinity (obtained from WAXD) for 1,4-two-arm PEO during heating at a rate of 0.5°C min^{-1} (a), and changes in the long periods (obtained from SAXS) of the two crystal populations of the 1,4-two-arm PEO during heating at the same rate (b).

inter-lamellar amorphous region, leading to a decrease in the crystallinity. According to the WAXD and DSC results for crystals formed at 48°C following a weight correction accounting for the coupling agents, it was determined that linear PEO (M_n = 2220) possesses 10% more crystallinity than the three two-arm PEOs.

4.3. Thermodynamic stability of the two-arm poly(ethylene oxide) crystals

The observation of two separated melting endotherms from DSC scans of 1,4-two-arm PEO crystallized at 48°C (Figs. 2 and 4) indicates the existence of two crystal populations. The lower endotherm shows a melting temperature nearly identical to that found for the linear PEO (M_n = 2220) (peak temperature at 54.5°C), while the second endotherm is approximately 1.1°C higher. This indicates that these two types of crystals possess different thermodynamic stabilities. A similar situation can also be found in the case of the 1,3-two-arm PEO (Figs. 3 and 4). We have speculated that the two melting temperatures of these two-arm PEOs may be associated with the existence of separate once-folded and extended OMC crystals. This speculation can be confirmed by Fig. 9. Upon heating the 1,4-two-arm PEO (at 0.5°C min^{-1} in the synchrotron X-ray experiments) after crystallization at 48°C, the development of crystallinity (obtained from WAXD) shown in Fig. 9(a) suggests that crystal melting consists of two steps: the first melting step starts at approximately 51°C and only 40% crystallinity remains at 54.5°C. This is an indication that one of the crystal populations has melted. The remaining crystal population is more stable and melts at 56.5°C during the second melting step.

The long period changes observed in SAXS results for the 1,4-two-arm PEO crystallized at 48°C (Fig. 9(b)) show that the smaller long period (17.3 nm), which is associated with the extended OMC crystals, decreases in scattering intensity and increases in long period starting at 51°C. This initially smaller long period crosses the larger long period (19.8 nm) at 52°C and reaches a plateau of 23.0 nm at 53°C. Above that temperature, this long period gently increases to 24.0 nm at 54.5°C. However, the scattering peak of the larger long period (19.8 nm), which is associated with once-folded OMC crystals, remains constant up to 53.0°C, after which a thickening process occurs up to 54.5°C. Above this temperature, only one broad scattering peak can be found with a gradual increase of the long period and a decrease of the scattering intensity until all of the crystals are molten at 56.5°C (the final long period is 26.5 nm). This indicates that crystals with the extended OMC are less stable than those with the once-folded OMC. Therefore, the conclusion may be made that the lower temperature melting endotherm corresponds to the melting of the extended OMC crystals whereas the higher melting temperature melting endotherm corresponds to the once-folded OMC crystals.

As previously reported, in the linear PEO (M_n = 4250) the once-folded chain crystals exhibit a melting temperature 5°C lower than that of the extended chain crystals. This difference in melting temperature is mainly attributed to two crystal populations with two lamellar thicknesses (13.7 versus 25.0 nm) [19–21]. For the two-arm PEOs, the lamellar crystal thicknesses of both OMCs are virtually identical and are similar to the lamellar thickness of linear the PEO (M_n = 2220). This causes the melting temperatures of the two-arm PEO crystals to be close to that of the ''parent'' linear PEO.

However, the study on linear LMW PEO revealed that their melting temperatures are not only dependent on the lamellar thickness but also on the number of folds per molecule [19–21]. When comparing the melting temperature of the extended chain PEO crystals to that of once-folded PEO crystals with the same lamellar thickness (for example, extended chain crystals of PEO (M_n = 2220) and once-folded chain crystals of PEO (M_n = 4440)), the former shows a melting temperature 3°C lower than the latter one (55.0 versus 58.0°C) [19–21]. This indicates that the extended chain crystals are less thermodynamically stable than the once-folded chain crystals with identical lamellar thicknesses. Note that, although the molecular weight distributions of these PEOs are narrow, they do not crystallize into perfect molecular crystals. In the present study, crystals with extended and once-folded OMCs have the same crystal

lamellar thickness and no hydrogen bonding can form between the chain ends. Therefore, the 1–1.5°C difference between the two endotherms of the 1,4- and 1,3-two-arm PEOs may imply a difference due to the configurational defect arrangements of the arms in the different OMCs on the PEO lamellar crystal surfaces. In other words, the arrangements of the defect layers change the surface free energy of these two PEOs. Experimental results seem to indicate that the surface free energy is higher for the crystals with the extended OMC than those with the once-folded OMC.

SAXS results of the 1,2-two-arm PEO which crystallizes at 48°C show only one relatively broad scattering peak with a relatively short correlation length. Its melting endothermic process possesses one dominant peak with a small shoulder. After comparison with the long periods of 1,4- and 1,3-two-arm PEO once-folded OMC crystals, it can be concluded that the long period of 20.4 nm for crystals of the 1,2-two-arm PEO is mainly associated with once-folded OMC crystals. Note that the 1,2-two-arm PEO possesses an angle of 60° between its two arms at the coupling agent. This structural feature may restrict the chains to forming crystals with purely extended OMC. It is conceivable that by changing the defect configurations from the 1,4- to 1,2-two-arm PEOs, the extended OMC becomes increasingly difficult to form while the once-folded OMC is more favorable. The once-folded OMC crystals of the 1,2- and 1,3-two-arm PEOs exhibit higher melting temperatures than those of the 1,4-two-arm PEO. One may speculate that the folds are relatively easier to form for the 1,2-two-arm PEO and thus are tighter than those in the 1,4-two-arm-PEO, namely a lower folded surface free energy.

5. Conclusion

In summary, upon crystallization of the two-arm PEO at relatively low undercoolings, two different nanoscopically separated OMCs may be identified for the subsequent crystals: the once-folded and extended OMCs. These OMCs were determined by combined SAXS and DSC experiments. It is interesting to note that the crystal structures of these OMCs are identical (WAXD results). Crystals with the extended OMC possess one defect layer between neighboring lamellae while those with the once-fold OMC include two defect layers, one above and one below the lamella. The appearance of these two OMCs is not only dependent on the crystallization conditions, but are also associated with the defect configurations of the two-arm PEO chains, namely the 1,4-, 1,3- and 1,2-two-arm positions. The crystals containing the extended OMC show a lower thermodynamic stability than those of the once-folded OMC.

Acknowledgements

This research was supported by the National Science Foundation (DMR-9617030). Research was carried out in part at the National Synchrotron Light Source at Brookhaven National Laboratories, which was supported by the US Department of Energy, Division of Material Science and Division of Chemical Sciences.

References

[1] Cheng SZD, Zhang A-Q, Chen J-H. J Polym Sci Polym Lett Ed 1990;28:233.
[2] Cheng SZD, Zhang A-Q, Chen J-H, Heberer DPJ. Polym Sci Polym Phys Ed 1991;29:287.
[3] Cheng SZD, Chen J-H, Zhang A-Q, Heberer DP. J Polym Sci Polym Phys Ed 1991;29:299.
[4] Cheng SZD, Chen J-H. J Polym Sci Polym Phys Ed 1991;29:311.
[5] Cheng SZD, Zhang A, Barley JS, Chen J, Habenschuss A, Zschack PR. Macromolecules 1991;24:3937.
[6] Cheng SZD, Chen J-H, Zhang A-Q, Barley JS, Habenschuss A, Zschack PR. Polymer 1992;33:1140.
[7] Cheng SZD, Chen J-H, Barley JS, Zhang A-Q, Habenschuss A, Zschack PR. Macromolecules 1992;25:1453.
[8] Cheng SZD, Wu SS, Chen J-H, Zhuo Q, Quirk RP, von Meerwall ED, Hsiao BS, Habenschuss A, Zschack PR. Macromolecules 1993;26:5105.
[9] Lee S-W, Chen E, Zhang A, Yoon Y, Moon BS, Lee S, Harris FW, von Meerwall ED, Hsiao BS, Verma R, Lando JB. Macromolecules 1996;29:8816.
[10] Kovacs AJ, Gonthier A. Colloid and Polym Sci 1972;250:530.
[11] Kovacs AJ, Gonthier A, Straupe C. J Polym Sci Polym Symp 1975;50:283.
[12] Kovacs AJ, Straupe C, Gonthier A. J Polym Sci Polym Symp 1977;59:31.
[13] Kovacs AJ, Straupe C. J Crystal Growth 1980;48:210.
[14] Kovacs AJ, Straupe C. Faraday Discuss Chem Soc 1979;68:225.
[15] Takahashi Y, Tadocoro H. Macromolecules 1975;6:672.
[16] Keller A, Cheng SZD. Polymer 1998;39:4461.
[17] Cheng SZD, Keller A. Ann Rev Mater Sci 1998;28:533.
[18] Chen E. PhD dissertation, Department of Polymer Science, The University of Akron, Akron, OH, 1998.
[19] Buckley CP, Kovacs AJ. Progr Colloid and Polym Sci 1975;58:44.
[20] Buckley CP, Kovacs AJ. Colloid ZZ Polym 1976;254:695.
[21] Cheng SZD, Wunderlich B. J Polym Sci Polym Phys Ed 1986;24:577.